Measurement of the Nonlinear Loss and Effective Free Carrier Lifetime in Silicon Microring Resonators

Karan Mehta, Ranjeet Kumar, Mehbuba Tanzid, David Gold, Haisheng Rong, and Richard Jones

***Abstract*—A methodology is presented to characterize the nonlinear absorption loss coefficient and the effective free carrier lifetime in silicon ring resonators at high intra-ring optical power density. The proposed methodology uses a continuous-wave pump-probe measurement to capture distortion-free transmission spectra in the regime of nonlinear absorption. The measured nonlinear loss coefficient using this method is 30–40% higher than that obtained with a single high-power continuous-wave laser. The pump-probe measurement also reveals that the optical loss sharply increases beyond ∼11.6 mW in the bus waveguide for the ring design with the highest quality-factor, most likely due to the saturation of trap states by electrons and holes generated by two-photon absorption.**

***Index Terms*—Free carrier absorption, nonlinear absorption, photonics integrated circuits, ring resonators, silicon photonics.**

I. Introduction

MICRORING resonators are versatile optical components used in a variety of different applications, from transceiver and sensing photonic integrated circuits (PICs) to external-cavity lasers on integrated photonics platforms. Microring modulators are preferrable to Mach-Zehnder modulators in transceiver PICs due to their smaller physical footprint, simpler driver design, and reduced power consumption [1]. Microring wavelength discrimination can be used as high quality-factor (Q) filters in single-wavelength narrow-linewidth lasers [2], to generate a frequency comb in multi-wavelength lasers [3], as on-chip Vernier tuning elements in tunable lasers [4], [5], and in optical (de)multiplexers [6]. Silicon photonics technology allows for low-loss integration of III-V gain material with silicon-on-insulator (SOI) waveguides using adiabatic tapers [7], [8]. Heterogeneous integration with passive alignment between III-V gain material and silicon microring resonators enables 300-mm wafer scale production of on-chip microring-resonator-coupled lasers [9], [10].

At high intra-ring optical power densities, nonlinear loss due to two-photon absorption (TPA) and free carrier absorption (FCA) degrades a ring resonator's performance by reducing the photon lifetime and causing wavelength hysteresis, thus limiting its capability for the above applications. Nonlinear optical absorption limits the performance of ring-resonator-coupled lasers in terms of the maximum output power, side-mode suppression ratio, and wavelength stability due to self-pulsing and hysteresis effects [2], [11], [12], [13]. In transceivers using ring modulators, wavelength hysteresis caused by self-heating causes eye closure and increases the bit error rate [14]. At high optical power densities, the reduction in the extinction ratio (ER) of ring modulators due to nonlinear absorption results in a lower optical modulation amplitude [15]. Therefore, it is important to accurately characterize the optical power-dependent nonlinear loss when designing high-power ring-resonator-coupled lasers and microring modulators.

The nonlinear loss in a ring waveguide can be measured using either continuous-wave (CW) or pulsed optical measurements. Pulsed pumped-probe measurements can directly estimate the free carrier lifetime, but they are less straightforward to carry out than CW measurements [16]. Furthermore, the use of CW measurements simplifies the extraction of the nonlinear loss coefficient by allowing the use of steady-state conditions when solving for the free carrier and photon densities. CW optical measurements can be used to indirectly extract the nonlinear loss and the effective free carrier lifetime from undistorted transmission spectra [17]. Previously reported CW measurements of the nonlinear loss in ring resonators have been made with a single laser, using distorted transmission spectra at high bus power [12], [18]. For the passive silicon microring resonators characterized in this manuscript, we find that measurements made with the pump-probe experimental setup yield different results compared to those made by sweeping the wavelength of a single high-power laser. There are significant differences in the measured ER and shift in the resonance wavelength of the ring resonators as a function of the bus power between the two sets of measurements, which suggests that the measurements made with a single laser significantly underestimate the optical loss due to nonlinear absorption.

Section II reviews the CW pump-probe measurement setup, and the methodology used to extract the nonlinear loss and effective free carrier lifetime from the measured optical spectra. The results in Section III indicate that the measurements made with a single high-power laser underestimate the nonlinear absorption coefficient by ∼40% compared to pump-probe measurements. Recent reports suggest that the Shockley-Read-Hall recombination lifetime in SOI waveguides is a function of the optical power circulating within the ring resonator [16], [19]. The optical loss due to FCA is proportional to the product of

Manuscript received 18 July 2023; revised 14 November 2023; accepted 11 January 2024. Date of publication 15 January 2024; date of current version 2 May 2024. *(Corresponding author: Karan Mehta.)*

The authors are with Intel Corporation, Santa Clara, CA 95054 USA (e-mail: karan.mehta@intel.com; ranjeet.kumar@intel.com; mihika.tanzid@intel.com; david.gold@intel.com; haisheng.rong@intel.com; richard.jones@intel.com).

Color versions of one or more figures in this article are available at https://doi.org/10.1109/JLT.2024.3354105.

Digital Object Identifier 10.1109/JLT.2024.3354105

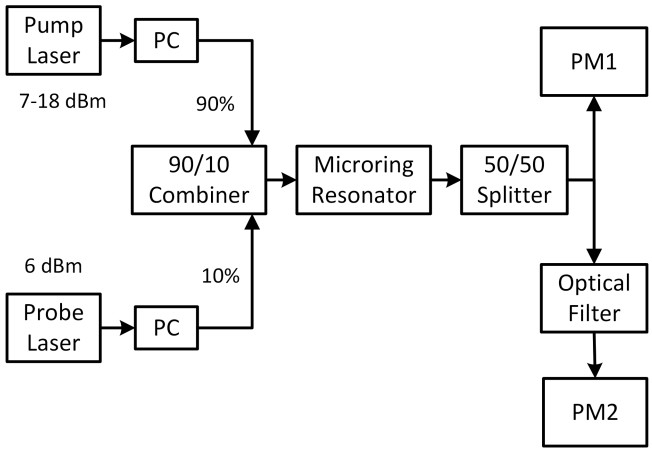

Fig. 1. Pump-probe experimental setup to characterize the nonlinear loss coefficient in microring resonators.

the effective free carrier lifetime (τ) and the FCA cross section (σ_{FCA}), thus making $\tau * \sigma_{\mathrm{FCA}}$ an important design parameter for ring resonators in high-power applications. Previous attempts to use a single value of τ and σ_{FCA} to fit the measured loss in silicon ring resonators underestimate the optical loss at high intracavity powers [18]. The experimental results presented in Section III support the hypothesis that the effective carrier lifetime in ring resonators increases with optical power, suggested to be due to the saturation of trap states by TPA-generated electrons and holes.

II. Measurement and Characterization Methodology

A. Experimental Setup

A simplified schematic of the experimental setup is shown in Fig. 1. The high-power pump laser is connected to the 90% input arm of the 90/10 combiner, and the probe laser is connected to the 10% input arm. Each of the lasers is connected to its own polarization controller (PC) before the combiner in order to align the polarization of input light waves with the device's polarization axis. The light from the output of the combiner is coupled into the ring resonator chip and coupled out of the through port to a 50/50 splitter. The splitter output is connected to a power meter (PM1) in one arm, and a bandpass optical filter followed by another optical power meter (PM2) in the second output arm. The optical losses due to coupling and the components in the optical link are accounted for when estimating the bus waveguide power ($\mathrm{P_{bus}}$) from the laser power.

The pump laser wavelength is aligned to one of the ring resonances at ~1318 nm by minimizing the power detected by PM1. The probe laser scans the resonance around 1321 nm with increasing wavelength. The filter passband was chosen to be from 1320 nm to 1322.5 nm to block the pump power at PM2.

B. Ring-Bus Designs and Waveguide Geometry

The three ring resonators discussed in this manuscript are fabricated with Intel's commercial 300-mm silicon photonics process. The ring resonators have a symmetric add-drop configuration with radii of 50 μm. The ring and bus waveguides are undoped. Each of the three rings have different bus-ring waveguide gaps which leads to different power cross-coupling coefficients ($\mathrm{k_d^2}$) and quality-factors. Rings R1, R2, and R3 have gaps of 0.36 μm, 0.32 μm, and 0.28 μm, which correspond to Q of 32k, 25k, and 19k, respectively. The simulated area of the ring waveguide's fundamental TE mode (σ) is 0.2 $\mu\mathrm{m}^2$; and the group index derived from the measured 1.41 nm free spectral range (FSR) is 3.93.

C. Measured Transmission Spectra

Fig. 2(a) shows the transmission spectra of ring R1 obtained by sweeping the wavelength of a single tunable laser for various bus powers. As $\mathrm{P_{bus}}$ increases, the resonance wavelength red-shifts according to a trade-off between thermo-optic and electro-refractive effects [20]. The measured spectra in Fig. 2(a) can be seen to become asymmetric and distorted at $\mathrm{P_{bus}}$ >10 mW. The wavelength detuning between the laser and the ring resonance changes with time during the measurement, resulting in the temperature (T) and TPA-generated free carrier concentration (N) in the ring resonator not being at steady-state during the laser wavelength sweep, i.e., $\partial N/\partial t$ and $\partial T/\partial t \neq 0$. The fraction of optical power coupled into the ring resonator is strongly dependent upon the detuning between the pump laser wavelength and the ring resonance wavelength [21], and the wavelength detuning changes with time during the wavelength sweep. The nonlinear absorption increases with $\mathrm{P_{bus}}$, which manifests as a reduction in the ER and an increase in the 3-dB resonance bandwidth ($\delta\lambda$).

Fig. 2(a) can be compared to the spectra measured with the pump-probe setup shown in Fig. 2(b). The pump-probe measurements yield symmetric and undistorted transmission spectra at high optical powers because the temperature and free carrier concentration in the ring resonator are dominated by the fixed-wavelength pump laser, while the low-power probe laser scans the transmission spectrum without significantly perturbing the ring waveguide's refractive index. Thus, $\partial N/\partial t$ and $\partial T/\partial t \approx 0$ in the pump-probe measurement. The low frequency ripples in the measured spectra are due to etalons originating from reflections in off-chip optical components.

D. Methodology to Characterize the Nonlinear Absorption Loss and Free Carrier Lifetime

Using the methodology derived by Xiao et al. [17], (1)–(4) are used to calculate the optical loss coefficient (α_{ring}) in symmetrically coupled add-drop microring resonators from parameters directly extracted from the measured transmission spectrum, such as the FSR, ER, and $\delta\lambda$, with the resonance bandwidth ($\delta\lambda$) being identical at the through and drop ports for the *symmetrically* coupled add-drop ring resonators studied here. The ER (dB) is measured at the through port.

$$\mathrm{T_0} = 10^{-\mathrm{ER}/10} \tag{1}$$

$$\mathrm{k_p^2} = 2\pi\delta\lambda\sqrt{\mathrm{T_0}}/FSR \tag{2}$$

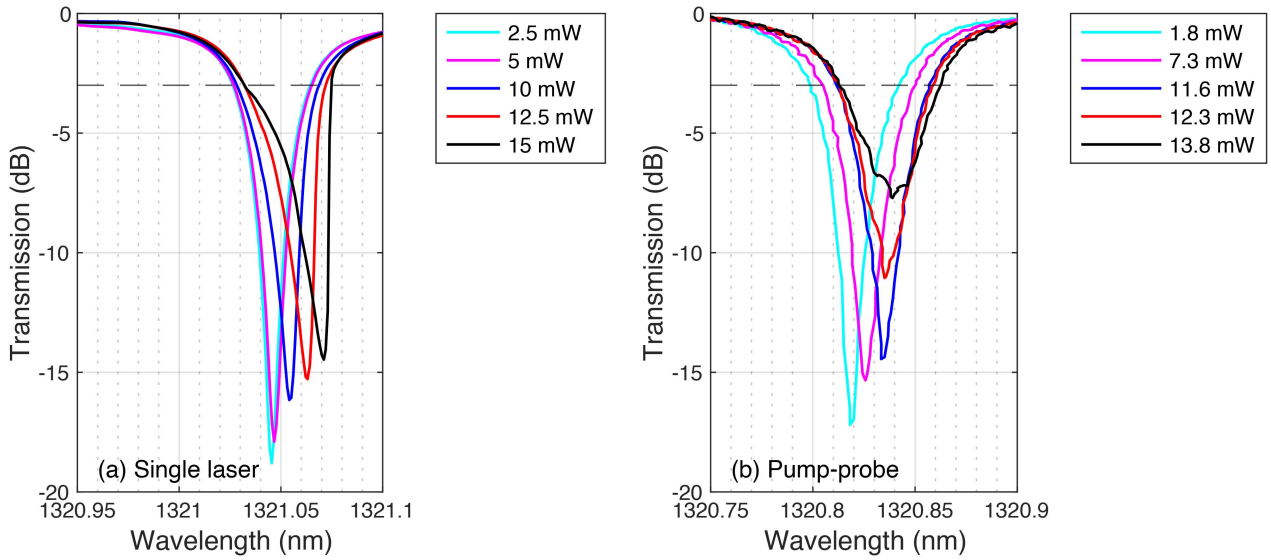

Fig. 2. Transmission spectra of ring R1 measured at bus powers from 1 mW to 15 mW with the (a) single laser and (b) pump-probe setups.

$$k_d^2 = \pi\delta\lambda\left(1-\sqrt{T_0}\right)/\mathrm{FSR} \tag{3}$$

$$\alpha_{ring} = -\log_e\left(1-k_p^2\right)/\left(2\pi R\right) \tag{4}$$

where T_0 is the linear extinction ratio, λ_0 is the ring resonance wavelength, k_p^2 is the fraction of intrinsic losses in the ring due to scattering, absorption, and bends, and k_d^2 is the fraction of optical power coupled out of the drop-port of the ring resonator of radius R.

As evident from Fig. 2(b), $\delta\lambda$ can be directly derived from the transmission spectra obtained with the pump-probe measurement, which allows (2) and (3) to be applied at all values of P_{bus}. With the single laser measurement, on the other hand, $\delta\lambda$ must be indirectly calculated at high P_{bus} since it cannot be directly measured due to nonlinear distortion. To infer $\delta\lambda$ at high power from the distorted transmission spectra, k_d^2 is first calculated at low power, where there is little nonlinear distortion. k_d^2 is then assumed to be constant for all values of P_{bus}. Since k_d^2 is known and the ER can be measured at high power, $\delta\lambda$ can subsequently be calculated by rearranging (3). For rings with critical or weak coupling, the optical loss coefficient can be estimated from a distorted transmission spectrum by using the low-power Q and the high-power ER [12], [22], but this coupling condition is not true for the rings characterized in this manuscript. Here, we take a more general approach by defining the ratio of the optical power in the ring resonator (P_{ring}) to P_{bus} as the power enhancement factor (B) [23]. For a symmetric add-drop ring resonator, B is calculated as per (5).

$$B = \frac{r^2\left(1-r^2\right)a^2}{\left(1-r^2a\right)^2} \tag{5}$$

$$r^2 = 1-k_d^2 \tag{6}$$

$$a^2 = 1-k_p^2 \tag{7}$$

The nonlinear loss coefficient in a ring resonator is a material, design, and process-dependent parameter when normalized to the intra-ring optical power density S_{ring} (mW/μm^2). S_{ring} depends on P_{bus} and the mode area of the ring waveguide (σ) as per (8).

$$S_{ring} = BP_{bus}/\sigma \tag{8}$$

The optical loss coefficient in a waveguide comprises of the linear loss coefficient and the nonlinear loss coefficients due to TPA and FCA, as expressed in (9)–(11) for steady-state conditions [24].

$$\alpha_{ring} = \alpha_{linear} + \alpha_{TPA} + \alpha_{FCA} \tag{9}$$

$$\alpha_{ring} = \alpha_{linear} + \beta S_{ring} + \left(\beta\tau\sigma_{FCA}/2h\nu\right)S_{ring}^2 \tag{10}$$

$$\alpha_{NL} = \alpha_{ring} - \alpha_{linear} \tag{11}$$

where $h\nu$ is the photon energy, β is the TPA coefficient in silicon, and α_{NL} is the nonlinear absorption loss coefficient. To simplify the analysis, hole and electron differences are ignored and an effective carrier lifetime, τ, and an effective FCA cross section σ_{FCA}, are used. By assuming the TPA coefficient β to be 5×10^{-13} cm/mW [25] and $\sigma_{0,FCA}$ of 1.04×10^{-17} cm^2 [26], α_{ring} is fitted versus S_{ring} as per (10) to obtain the linear waveguide loss (α_{linear}) and τ.

III. Results and Discussion

A. Comparison of Nonlinear Loss Measured Using the Single Laser and Pump-Probe Setups

The nonlinear loss coefficient (α_{NL}) in each of the three rings was calculated using (11) across a range of input powers with both the single laser and pump-probe measurements. Fig. 3 indicates that the nonlinear absorption loss coefficient derived with the pump-probe measurement is 30–40% higher than that obtained with a single laser for all three rings. Consequently, the effective free carrier lifetime τ derived with the pump-probe measurement is 21 ± 1 ns, compared to 13 ± 1 ns when measured

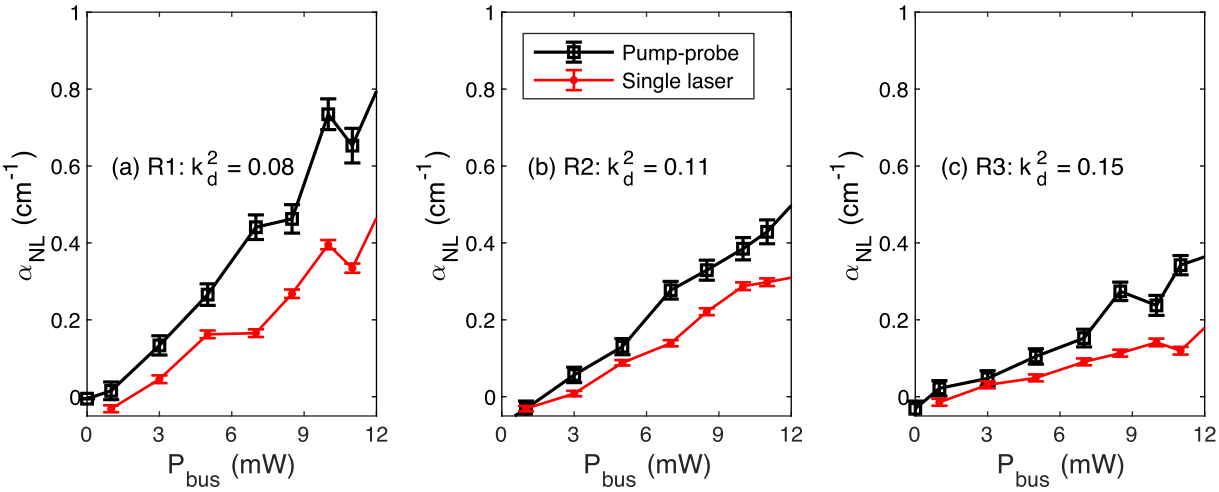

Fig. 3. Nonlinear absorption loss coefficient as a function of the bus power for ring resonators (a) R1, (b) R2, and (c) R3 with pump-probe and single laser measurements up to a bus power of 12 mW.

TABLE I
PARAMETERS OBTAINED WITH PUMP-PROBE MEASUREMENTS

Ring	Gap (μm)	k_d^2	α_{linear} (cm^{-1})	τ (ns)	Q	B
R1	0.36	0.082	0.85	20	32k	8.3
R2	0.32	0.107	0.8	21	25k	7.1
R3	0.28	0.149	1.06	22	19k	5

TABLE II
PARAMETERS OBTAINED WITH A SINGLE LASER

Ring	Gap (μm)	k_d^2	α_{linear} (cm^{-1})	τ (ns)	Q	B
R1	0.36	0.091	0.63	14	33k	8.2
R2	0.32	0.113	0.51	13	25k	6.9
R3	0.28	0.156	0.72	12	18k	4.7

with a single laser. The loaded Q ($Q = \lambda_0 / \delta\lambda$) and the power buildup factors (B) at low power are shown in Tables I and II. As the waveguide gap reduces from R1 to R3, the coupling loss increases, which is why R3 has the lowest Q and B. We suspect that ring R3 has the highest linear loss because of increased scattering loss at the coupler.

As seen in Fig. 3, the nonlinear loss for a given bus power is reduced when the coupling coefficient of the ring resonator increases due to a decrease in ring Q, power buildup factor (B), and intra-ring power. Thus, the ring resonator can be made more tolerant to high P_{bus} by increasing k_d^2, but this comes at the cost of a wider resonance bandwidth, which can adversely affect its use in the applications described in Section I.

The nonlinear loss depends on the optical power density within the ring waveguide (S_{ring}), the rib waveguide design, the fabrication process, and the SOI substrate. The nonlinear loss as a function of S_{ring} should be similar for the three rings, since they were all fabricated with the same process on the same wafer with the same waveguide design. Fig. 4(a), (b) shows that both sets of measurements are consistent with this physical model, as the three rings have similar nonlinear loss versus intra-ring power density.

These measurements were reproduceable with the extinction ratio being within ±0.1 dB and the measured resonance bandwidth within ±1 pm over consecutive measurements. These tolerances in the measurement apparatus were used to calculate the error bars in Figs. 3 and 4, as per (2) and (4).

As seen in Figs. 3 and 4, ring resonators with higher Q are more susceptible to nonlinear absorption because they have greater intra-cavity optical power density S_{ring} for a given P_{bus} due to higher power buildup factor B. The following analyses in Section III-B and III-C are focused on Ring R1 because it has the highest Q and shows the greatest optical loss due to nonlinear absorption.

B. Intracavity Optical Power Versus Bus Power

The optical power in the bus and ring waveguides are related through the power buildup factor (B), where $B = P_{ring}/P_{bus}$. For the symmetric add-drop ring resonator R1, B can be calculated using (5), and it is plotted versus P_{bus} in Fig. 5 along with the intra-ring power (P_{ring}). The power buildup factor slowly decreases as the bus power is increased, due to the increase in nonlinear loss. A peak intra-ring power is reached at P_{bus} ~11.6 mW, beyond which the intra-ring power and the power buildup factor sharply decrease. The oscillatory behavior of α_{NL} beyond ~350 mW/μm^2 in Fig. 4(b) corresponds to the onset of saturation of trap states.

C. Increase in FCA Loss at High-Power Due to Saturation of Trap States

The total optical loss coefficient of Ring R1 is plotted versus P_{bus} in Fig. 6(a). The solid line in Fig. 6(a) indicate α_{ring} derived from the measured transmission spectra, and the dotted lines depict the loss coefficient obtained by fitting (10) to the measured data. A constant FCA cross section ($\sigma_{0,FCA}$) of 1.04×10^{-17} cm^2 is assumed up to a bus power of 11.6 mW [26], and the fit yields an effective carrier lifetime of 20 ns and a linear loss coefficient of 0.83 cm^{-1}. However, to fit the data to (10) at bus powers exceeding 11.6 mW, $\tau * \sigma_{FCA}$ must also increase with

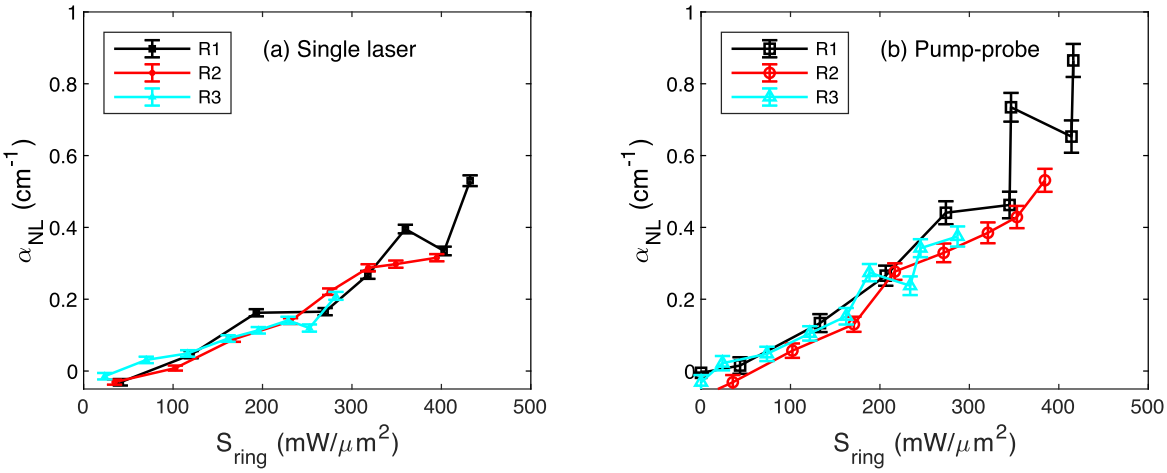

Fig. 4. Nonlinear absorption loss coefficient versus the intra-ring power density for ring resonators R1, R2, and R3 with the (a) single laser and (b) pump-probe measurements setups.

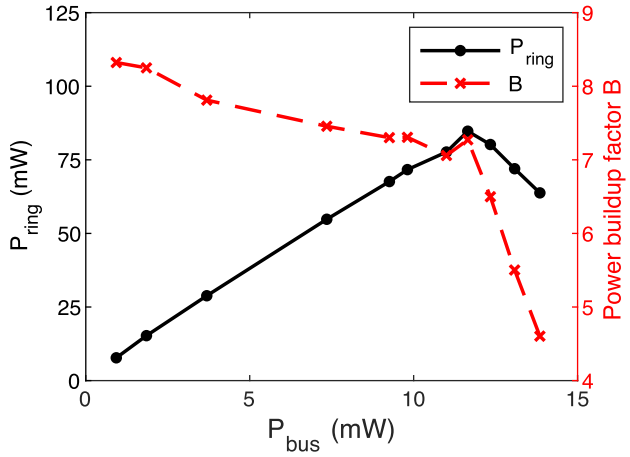

Fig. 5. Intra-ring optical power and the power buildup factor versus the optical power in the bus waveguide.

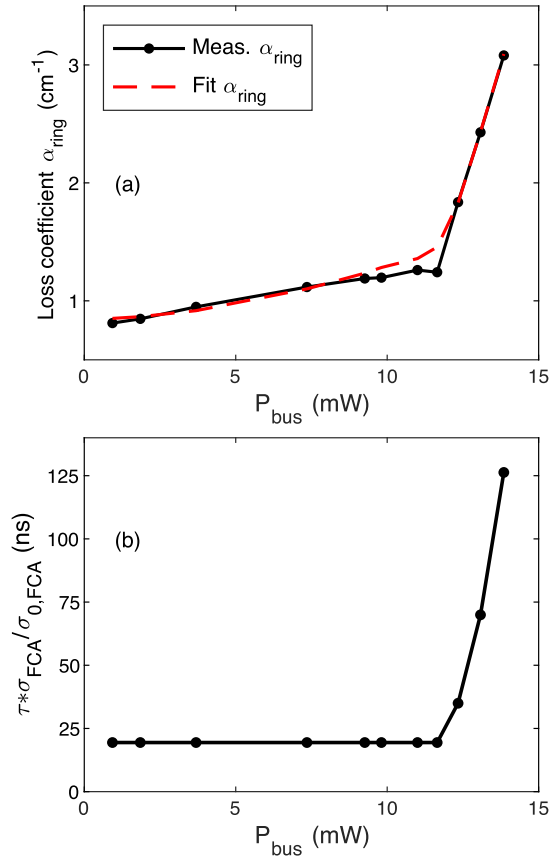

Fig. 6. (a) Optical loss coefficient in the ring waveguide and (b) the product of the FCA cross section and effective carrier lifetime versus the optical power in the bus waveguide.

P_{bus}, as shown in Fig. 6(b). When fitting the measured data to (10), only P_{ring}, α_{ring}, and $\tau*\sigma_{FCA}$ are assumed to depend on P_{bus}.

The effective carrier lifetime (τ) denotes the timescale of the interaction between free carriers and the optical mode. In this simplified analysis, the effective lifetime shown in Fig. 6(b) assumes that the TPA-generated steady-state electron and hole concentrations are equal, and that the electron and hole recombination lifetimes, FCA cross sections, and diffusion lengths are also equal. We note the limitation of using this simplification, here the effective lifetime is used as a metric to determine the maximum CW power handling capability of a ring resonator, and it should not be used to quantify the real carrier lifetimes of electrons and holes, which would require transient measurements.

The effective free carrier lifetime comprises of the bulk recombination lifetime, the sidewall recombination lifetime, and the carrier transit time [26]. The bulk lifetime is determined by impurities in the silicon rib waveguide and is sensitive to the doping concentration in the waveguide. The sidewall recombination lifetime is governed by the energy levels and densities of surface trap states at the interface between the silicon core and silicon dioxide cladding [19], which depends on the etch and passivation recipes used in device fabrication. The transit time depends on the carrier mobility, the bulk recombination

lifetime, and the cross-sectional profiles of the optical mode and the waveguide [26].

Based on transient pump-probe measurements, Novarese et al. reported that the electron lifetime in silicon microrings increased by over a factor of 3 as the laser power increased from 11 dBm to 18 dBm [16]. Using simulations, they also showed that the free carrier lifetime can increase by over an order of magnitude within 80 mW of intra-ring power [19]. This is consistent with the data shown in Fig. 6. The proposed reason for the increase in the carrier lifetime at high optical powers is that trap states get saturated with TPA-generated free carriers.

IV. Conclusion

Ring resonators are used as integrated photonics building blocks in a range of devices such as filters, lasers, modulators, detectors, and (de)multiplexers. In this paper, we demonstrate a methodology to accurately measure the maximum power handling capability of ring resonators using a continuous-wave pump-probe technique. Nonlinear optical absorption, which increases significantly above a threshold value, fundamentally limits the maximum power handling capacity of ring-based photonic integrated circuits.

Improvements in microring power handling can be achieved using a variety of different methods. Reverse-biasing a silicon waveguide has been shown to reduce FCA loss by sweeping carriers out of the waveguide [27], thus reducing the optical loss while simultaneously preventing trap states from getting saturated. Where reverse-biasing the ring waveguide is not an option, the saturation of trap states can be deferred to higher bus powers by increasing the mode area to reduce the optical power density in the ring, and by increasing the power coupling coefficient between the ring and bus waveguides to reduce the optical power buildup factor in the resonator. Lastly, silicon nitride waveguides have orders of magnitude lower nonlinear absorption than silicon waveguides, which makes this platform an attractive option for high-power integrated photonics applications [12].

Acknowledgment

The authors would like to thank Meer Sakib for assistance with setting up the test equipment, Duanni Huang and Yuliya Akulova for technical discussions, and their colleagues in Intel Fab 11x, NM, USA for their help with device fabrication.

References

[1] J. Sun, R. Kumar, M. Sakib, J. B. Driscoll, H. Jayatilleka, and H. Rong, "A 128 Gb/s PAM4 silicon microring modulator with integrated thermo-optic resonance tuning," *J. Lightw. Technol.*, vol. 37, no. 1, pp. 110–115, Jan. 2019.

[2] T. Kita, R. Tang, and H. Yamada, "Narrow spectral linewidth silicon photonic wavelength tunable laser diode for digital coherent communication system," *IEEE J. Sel. Topics Quantum Electron.*, vol. 22, no. 6, pp. 23–34, Nov./Dec. 2016.

[3] Y. Zhang et al., "Quantum dot SOA/silicon external cavity multi-wavelength laser," *Opt Exp.*, vol. 23, no. 4, pp. 4666–4671, 2015.

[4] J. C. Hulme, J. K. Doylend, and J. E. Bowers, "Widely tunable Vernier ring laser on hybrid silicon," *Opt Exp.*, vol. 21, no. 17, pp. 19718–19722, 2013.

[5] P. A. Morton et al., "Integrated coherent tunable laser (ICTL) with ultra-wideband wavelength tuning and sub-100 Hz lorentzian linewidth," *J. Lightw. Technol.*, vol. 40, no. 6, pp. 1802–1809, Mar. 2022.

[6] A. Vorckel, M. Monster, W. Henschel, P. H. Bolivar, and H. Kurz, "Asymmetrically coupled silicon-on-insulator microring resonators for compact add-drop multiplexers," *IEEE Photon. Technol. Lett.*, vol. 15, no. 7, pp. 921–923, Jul. 2003.

[7] S. Dhoore, S. Uvin, D. Van Thourhout, G. Morthier, and G. Roelkens, "Novel adiabatic tapered couplers for active III–V/SOI devices fabricated through transfer printing," *Opt. Exp.*, vol. 24, no. 12, pp. 12976–12990, 2016.

[8] M. Lamponi et al., "Low-threshold heterogeneously integrated InP/SOI lasers with a double adiabatic taper coupler," *IEEE Photon. Technol. Lett.*, vol. 24, no. 1, pp. 76–78, Jan. 2012.

[9] H. Park et al., "Device and integration technology for silicon photonic transmitters," *IEEE J. Sel. Topics Quantum Electron.*, vol. 17, no. 3, pp. 671–688, May/Jun. 2011.

[10] B. Liu, A. Shakouri, and J. E. Bowers, "Passive microring-resonator-coupled lasers," *Appl. Phys. Lett.*, vol. 79, no. 22, pp. 3561–3563, Nov. 2001.

[11] T. J. Johnson, M. Borselli, and O. Painter, "Self-induced optical modulation of the transmission through a high-Q silicon microdisk resonator," *Opt. Exp.*, vol. 14, no. 2, pp. 817–831, 2006.

[12] C. Xiang et al., "Effects of nonlinear loss in high-Q Si ring resonators for narrow-linewidth III-V/Si heterogeneously integrated tunable lasers," *Opt. Exp.*, vol. 28, no. 14, pp. 19926–19936, 2020.

[13] T. K. Liang and H. K. Tsang, "Role of free carriers from two-photon absorption in Raman amplification in silicon-on-insulator waveguides," *Appl. Phys. Lett.*, vol. 84, no. 15, pp. 2745–2747, Apr. 2004.

[14] C. Sun et al., "A 45 nm CMOS-SOI monolithic photonics platform with bit-statistics-based resonant microring thermal tuning," *IEEE J. Solid-State Circuits*, vol. 51, no. 4, pp. 893–907, Apr. 2016.

[15] M. de Cea, A. H. Atabaki, and R. J. Ram, "Power handling of silicon microring modulators," *Opt. Exp.*, vol. 27, no. 17, pp. 24274–24285, 2019.

[16] M. Novarese, S. Romero-Garcia, J. Bovington, and M. Gioannini, "Dynamics of free carrier absorption and refractive index dispersion in Si and Si/PolySi microrings," *IEEE Photon. Technol. Lett.*, vol. 35, no. 8, pp. 450–453, Apr. 2023.

[17] S. Xiao, M. H. Khan, H. Shen, and M. Qi, "Modeling and measurement of losses in silicon-on-insulator resonators and bends," *Opt. Exp.*, vol. 15, no. 17, pp. 10553–10561, 2007.

[18] G. Priem, P. Dumon, W. Bogaerts, D. Van Thourhout, G. Morthier, and R. Baets, "Optical bistability and pulsating behaviour in Silicon-on-Insulator ring resonator structures.," *Opt. Exp.*, vol. 13, no. 23, pp. 9623–9628, 2005.

[19] M. Novarese, S. R. Garcia, S. Cucco, D. Adams, J. Bovington, and M. Gioannini, "Study of nonlinear effects and self-heating in a silicon microring resonator including a Shockley-Read-Hall model for carrier recombination," *Opt. Exp.*, vol. 30, no. 9, pp. 14341–14357, 2022.

[20] L.-W. Luo, G. S. Wiederhecker, K. Preston, and M. Lipson, "Engineering optical bistability in silicon ring resonators," in *Proc. Laser Appl. to Photonic Appl.*, 2011, Paper CWC4.

[21] T. Carmon, L. Yang, and K. J. Vahala, "Dynamical thermal behavior and thermal self-stability of microcavities," *Opt. Exp.*, vol. 12, no. 20, pp. 4742–4750, 2004.

[22] S. M. Spillane, T. J. Kippenberg, O. J. Painter, and K. J. Vahala, "Ideality in a fiber-taper-coupled microresonator system for application to cavity quantum electrodynamics," *Phys. Rev. Lett.*, vol. 91, no. 4, Jul. 2003, Art. no. 43902.

[23] J. Heebner, R. Grover, and T. Ibrahim, Eds., "Optical microresonator theory," in *Optical Microresonators: Theory, Fabrication, and Applications*. Berlin, Germany: Springer, 2008, pp. 83–85.

[24] H. Rong, A. Liu, R. Nicolaescu, M. Paniccia, O. Cohen, and D. Hak, "Raman gain and nonlinear optical absorption measurements in a low-loss silicon waveguide," *Appl. Phys. Lett.*, vol. 85, no. 12, pp. 2196–2198, Sep. 2004.

[25] Q. Lin, J. Zhang, G. Piredda, R. W. Boyd, P. M. Fauchet, and G. P. Agrawal, "Dispersion of silicon nonlinearities in the near infrared region," *Appl. Phys. Lett.*, vol. 91, no. 2, Jul. 2007, Art. no. 021111.

[26] R. Claps, V. Raghunathan, D. Dimitropoulos, and B. Jalali, "Influence of nonlinear absorption on Raman amplification in Silicon waveguides," *Opt. Exp.*, vol. 12, no. 12, pp. 2774–2780, 2004.

[27] R. Jones et al., "Net continuous wave optical gain in a low loss silicon-on-insulator waveguide by stimulated Raman scattering," *Opt. Exp.*, vol. 13, no. 2, pp. 519–525, 2005.